Monotonic Limiters for a Second-Order Finite-Volume Advection Scheme Using Icosahedral-Hexagonal Meshes

RASHMI MITTAL AND WILLIAM C. SKAMAROCK

National Center for Atmospheric Research, Boulder, Colorado*

(Manuscript received 14 May 2010, in final form 26 July 2010)

ABSTRACT

An assessment of a recently developed (by Miura) second-order numerical advection scheme for icosahedral-hexagonal grids on the sphere is presented, and the effects of monotonic limiters that can be used with the scheme are examined. The cases address both deformational and nondeformational flow and continuous and discontinuous advected quantities; they include solid-body rotation of a cosine bell and slotted cylinder, and moving dynamic vortices. The limiters of Zalesak, Dukowicz and Kodis, and Thuburn are tested within this numerical scheme. The Zalesak and Thuburn limiters produce solutions with similar accuracy, and the Thuburn limiter, while computationally less expensive per time step, results in more stringent stability conditions for the overall scheme. The Dukowicz limiter is slightly more diffusive than the other two, but it costs the least.

1. Introduction

Spherical icosahedral-hexagonal grids are potential candidates for next-generation atmospheric models because they avoid the latitude–longitude grid pole problem and allow easier parallel computing. For global models, the problem of performing accurate tracer transport has received considerable attention, and there are a number of numerical schemes available for simulating advection on regular latitude–longitude grids. However, the solution of the advection problem on icosahedral-hexagonal grids has not received as much attention because of the complexity in extending schemes developed for regular latitude–longitude grids to the icosahedral-hexagonal grid geometry.

Miura (2007) developed an upwind-biased finite-volume scheme for icosahedral hexagonal meshes that is regarded as a simplification of the remapping scheme of Lipscomb and Ringler (2005) and Yeh (2007). Miura's scheme is second-order accurate, and the method was shown to be stable and computationally simple but has only been tested using the solid-body rotation of a cosine bell. A more comprehensive assessment of this scheme is needed to evaluate its viability for global modeling. In our study, Miura's method is tested using a series of cases including solid-body rotation of a cosine bell and a slotted cylinder and a deformational-flow test case using dynamic translating vortices (Nair and Jablonowski 2008).

Two desirable properties of advection schemes are conservation and monotonicity. Miura's scheme is a finite-volume scheme, and it is locally and globally conservative by design. For conservative finite-volume schemes, monotonicity can be achieved either by modifying the tracer value at the interfaces, where it is used to compute the flux, or by adjusting the fluxes after they are computed. We study the behavior of three different monotonicity constraints: Zalesak [1979; flux-corrected transport (FCT)], van Leer [1977; extended to multiple dimensions by Dukowicz and Kodis (1987), henceforth DK87], and Thuburn (1996, henceforth T96). These three limiters are suitable for unstructured grids and can easily be used in icosahedral-hexagonal grid geometries. They differ significantly in their implementation. The FCT limiter renormalizes a higher-order corrective flux to maintain monotonicity, whereas the T96 and DK87 limiters modify the interfacial tracer values such that the resultant flux maintains monotonicity. DK87 and T96 use different approaches to estimate the tracer values on the cell faces.

---

* The National Center for Atmospheric Research is sponsored by the National Science Foundation.

Corresponding author address: Rashmi Mittal, Mesoscale and Microscale Meteorology, National Center for Atmospheric Research, P.O. Box 3000, Boulder, CO 80301-3000.
E-mail: mittal@ucar.edu

DOI: 10.1175/2010MWR3503.1

2. Numerical scheme

The advection equation for scalar variables in atmospheric models can be expressed as

$$\frac{\partial \rho q}{\partial t} + \nabla \cdot (\rho q \mathbf{V}) = 0, \tag{1}$$

where $\partial/\partial t$ is the local time derivative, $\mathbf{V}$ is the velocity field, ρ is the fluid density, and q represents the tracer concentration. On applying Gauss–Green's theorem and integrating in time, the discrete form Eq. (1) may be written as

$$(\rho q)_i^{t+\Delta t} = (\rho q)_i^t - \frac{1}{A_i}\sum_{n=1}^{N} F_n(\rho, \mathbf{V}, q, l), \tag{2}$$

where $(A\rho q)_i$ is the mass of tracer q inside the polygon of area A_i, q is the mean tracer mixing ratio, and F_n is the flux of tracer mass through the nth face with length l of the N-sided polygon over the time step Δt.

The numerical method of Miura (2007) consists of the following steps: 1) determine the linear reconstruction of tracer field q for each cell, 2) compute the fluxes at each cell face by spatial integration over the reconstruction as determined by the velocity field and time step, and 3) update the scalar mass using Eq. (2).

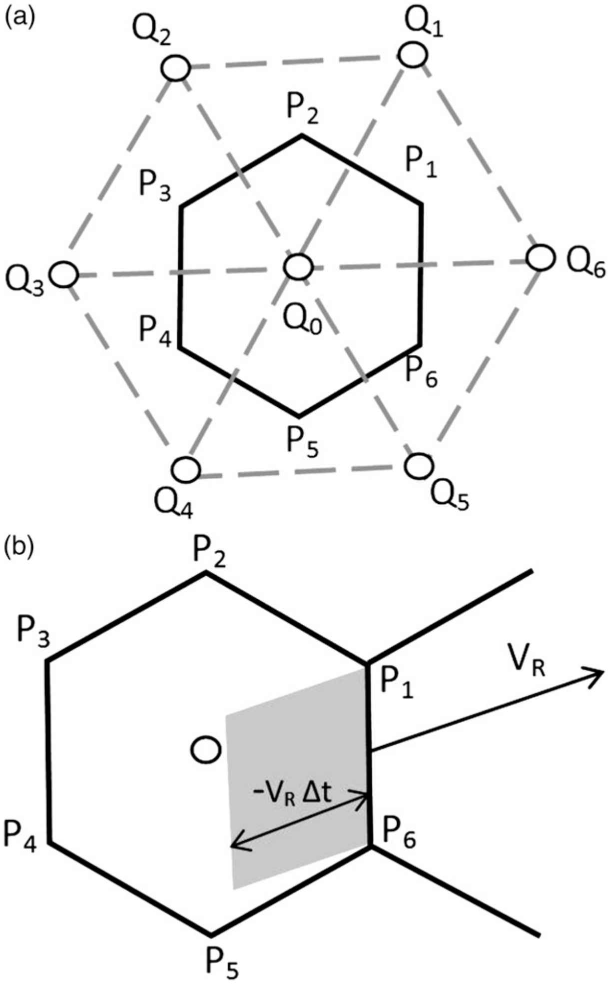

FIG. 1. Schematic describing (a) the grid and (b) the mass flux calculation.

For the linear reconstruction of the tracer field, consider a cell as shown in Fig. 1a, where the center of the cell is Q_0, and $Q_1, \ldots, Q_6$ represent the centers of the nearest neighboring cells. The cell average mixing ratios are defined at these cell centers as $q_0, q_1, \ldots, q_6$. The vertices of the cell with center Q_0 are represented by $P_1, \ldots, P_6$. The tracer field reconstruction for the cell is obtained on a plane tangent to the sphere at Q_0 with the neighboring points projected onto the plane as described in Lipscomb and Ringler (2005). The reconstruction function $q(x, y)$ is defined as

$$q(x, y) = q_0(x_0, y_0) + (x - x_0)\overline{q}_x + (y - y_0)\overline{q}_y, \tag{3}$$

where (x_0, y_0) represents the coordinates of point Q_0 and $\overline{q}_x$ and $\overline{q}_y$ are the average gradients in the cell. The average gradient value in a cell is computed as the area average over the gradients computed for the six triangles centered on $P_1, \ldots, P_6$ (viz., $\triangle Q_0Q_1Q_2$, $\triangle Q_0Q_2Q_3, \ldots$, $\triangle Q_0Q_6Q_1$, where $\triangle$ denotes a triangle):

$$\overline{q}_x = \frac{\sum_{i=1}^{6} q_x\big|_i \mathrm{Area}(\triangle Q_0Q_iQ_{i+1})}{\sum_{i=1}^{6}\mathrm{Area}(\triangle Q_0Q_iQ_{i+1})} \quad \text{and}$$

$$\overline{q}_y = \frac{\sum_{i=1}^{6} q_y\big|_i \mathrm{Area}(\triangle Q_0Q_iQ_{i+1})}{\sum_{i=1}^{6}\mathrm{Area}(\triangle Q_0Q_iQ_{i+1})}, \tag{4}$$

where the index $i + 1$ is cyclic and $q_x|_i$ and $q_y|_i$ represent the gradient components in each of these six triangles. Our approach is the same as used by Yeh (2007) with the only exception being that we use area averaging. Last, the flux computation for each edge follows Miura's (2007) approach in which the tracer mass fluxes may be written as

$$F_n = \rho_n q_n l_n(\mathbf{v}_R \cdot \hat{\mathbf{n}})\Delta t, \tag{5}$$

where $\mathbf{v}_R$ is the velocity at the midpoint R of the edge n, $\hat{\mathbf{n}}$ represents the unit vector normal to the edge, l is the length of the edge, and ρ and q are the mean values of the density and tracer mixing ratio for the parallelogram (Fig. 1b) computed from the reconstruction function (for a linear reconstruction, this is the function evaluated at the center of the parallelogram). The flux represents the mass of q advected through the edge over the time interval Δt. This formulation leads to a conservative scheme because the same flux is used to update both cells sharing the edge. The scheme is formally second-order accurate.

To preserve monotonicity, we have implemented gradient limiting by DK87, FCT (Zalesak 1979), and the multidimensional flux limiter of T96, which was also used by Miura (2007). FCT first uses the monotonic but diffusive first-order upwind scheme to advect the field followed by adding a compensating antidiffusive flux that reduces the numerical error. FCT limits these antidiffusive fluxes before they are applied, so that no unphysical extrema are created in the solution. T96 and DK87 involve only one step, and intermediate values of diffusive fluxes are not computed. In these two methods the interfacial values of the tracer field used in the flux calculations are constrained such that the resulting fluxes are monotonic. The T96 limiter examines the tracer values in the neighboring cells to define the minimum and maximum permitted values of the interfacial mixing ratios on the cell faces. The DK87 scheme limits the slopes in the reconstruction such that monotonicity is maintained. This scheme ensures that the reconstructions are monotonic across cell boundaries (in one dimension), but it does not guarantee monotinicity in two dimensions.

3. Test-case results

The experiments are performed at five different horizontal resolutions corresponding to levels 4–8 in Thuburn (1997) that have 642, 2562, 10 242, 40 962, and 163 842 cells on the sphere with radius a equal to 6371.229 km and average cell-center spacings of approximately 960, 480, 240, 120 and 60 km, respectively. The solid-body rotation wind component in these test cases is chosen such that one complete revolution around the globe occurs in 12 days with the angle of rotation equal to 0. The results are insensitive to the rotation angle. The L_∞ and L_2 error estimates (Williamson et al. 1992) are plotted for the test cases.

a. Nondeforming flow: Solid-body rotation

The transport of a cosine bell by a solid-body rotation flow field is given in Williamson et al. (1992). It is the only case described in Miura (2007). The cosine bell is given by

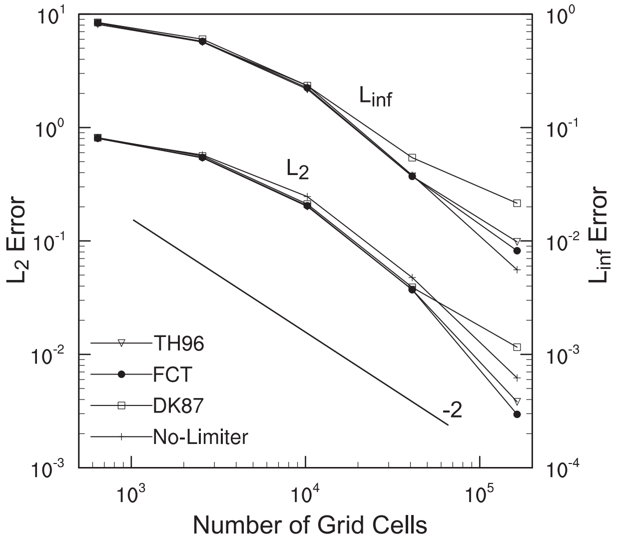

FIG. 2. The L_∞ and L_2 error norms for the solid-body rotation of the cosine bell with and without limiters. The norms are computed after one revolution of the sphere.

$$q(\lambda,\varphi)=\begin{cases}\dfrac{1}{2}[1+\cos(\pi r/R)], & \text{if} \quad r<R\\ 0 & \text{if} \quad r\geq R\end{cases}, \qquad (6)$$

where r represents the great circle distance from the center of the cosine bell, $(\lambda_0, \varphi_0) = (3\pi/2, 0)$, and the bell radius R is $7\pi a/64$.

The global error norms for the unlimited and limited versions of Miura's scheme are shown in Fig. 2. We used a fixed time step of 900 s in these tests. These schemes converge at a rate of higher than second order for this case, especially at higher resolutions or where the CFL number is higher. The DK87 limiter is more diffusive than the other limiters and the effect is most noticeable in the magnitude of L_∞ norm, which is higher in this test case. Also, as observed by Miura (2007), the L_2 error norms are appreciably reduced and higher convergence rates are obtained when monotonic limiters are used, especially with the T96 and FCT limiters.

Numerical transport schemes for the sphere have also been tested with the transport of a slotted cylinder in a solid-body rotation flow field (Lipscomb and Ringler 2005). This numerical experiment assesses the ability of limiters to handle discontinuities in the tracer profile. The cylinder has a tracer value of 1, and the tracer value is 0 outside the cylinder ($r \geq R$) as well as inside the slot. A slot of width $R/2$ and length $3R/2$ is used. The results depicted in Fig. 3 show that all of the limiters successfully remove the oscillations produced by the unlimited numerical scheme. The DK87 limiter is the most diffusive. The FCT limiter best captures the minimum in the

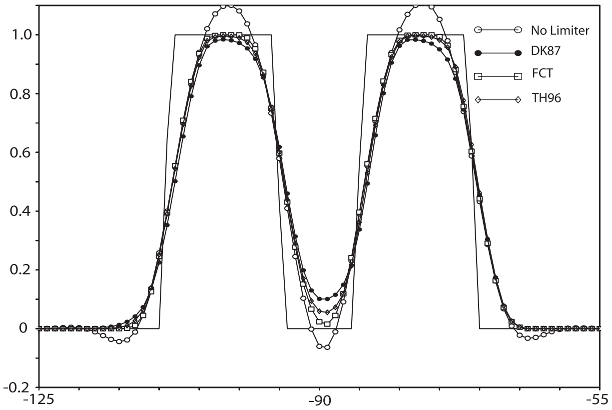

FIG. 3. One-dimensional cross section through the slotted cylinder after one revolution of the sphere.

slot and gives the lowest error norms of the three limiters. The L_2 error norms (not shown) indicate approximately first-order convergence for all schemes, as expected.

It was also observed by Miura (2007) that the global error increases when increasing the number of time steps (decreasing the time step) in the model integration. We observe the same behavior in our tests.

b. *Deformational flow with moving vortices*

In this test case described in Nair and Jablonowski (2008), solid-body rotation and a deformational flow field are combined to form moving vortices over the surface of the sphere. The deforming vortices lie on diametrically opposite sides of the sphere and move along a predetermined great circle trajectory. In one revolution around the sphere, the initially smooth scalar field develops strong gradients. The initial field is described as

$$q(\lambda', \theta', 0) = 1 - \tanh\left[\frac{\rho}{\delta}\sin(\lambda')\right], \qquad (7)$$

where (λ', θ') corresponds to the location of a point on the sphere, which has been rotated such that the vortex centers lie at the North and South Poles in the (λ', θ') system. The transformation relation between the rotated and unrotated system is given in the appendix of Nair et al. (1999). As in Nair and Jablonowski (2008), the deformational flow parameters are chosen as $\rho = 3$ and $\delta = 5$ and the time for a complete rotation is 12 days. The initial and final locations of the center of the two developing vortices lie on the equator at ±90° longitude in the unrotated system.

Figure 4 shows the analytic and simulated tracer field produced by the unlimited scheme at grid level 6 (10 242 cells, ~240-km cell spacing) on the sphere. The results look very similar to Figs. 4b,c of Nair and Jablonowski (2008) in which a semi-Lagrangian advection scheme on regular latitude–longitude grids is used. Both the unlimited and limited schemes successfully reproduce the

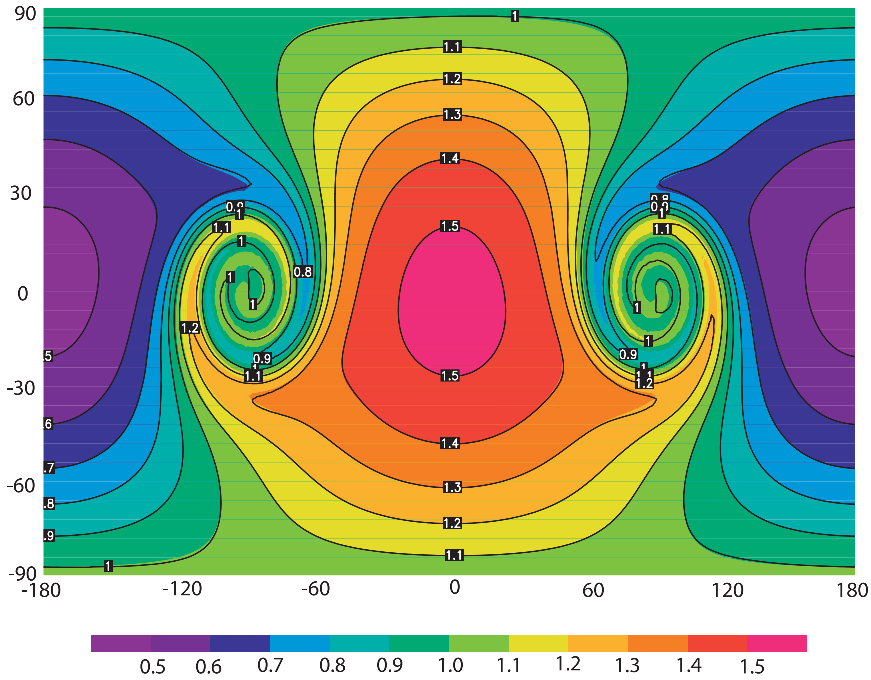

FIG. 4. Tracer field for the dynamic vortex case computed using the unlimited scheme. The analytic solution is shaded, and the numerical solution is contoured.

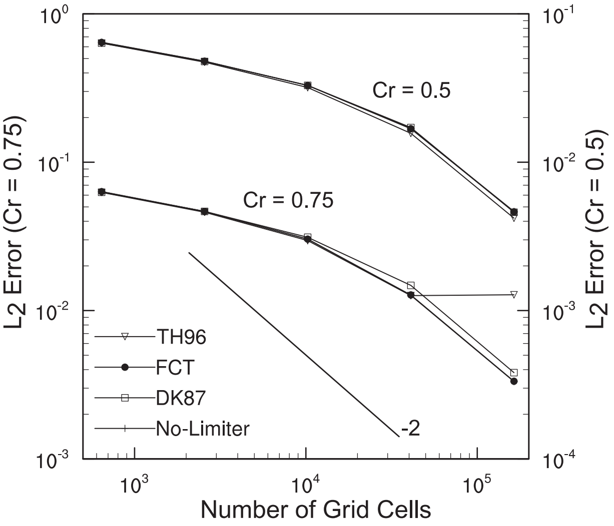

FIG. 5. The L_2 error norms from the dynamic vortex test case with and without limiters at Courant number ~0.75 and ~0.5.

highly deformed vortices. One outcome of this case is that the scheme using the T96 limiter could not maintain the convergence order at high Courant number (Fig. 5). The reason for this result is that the T96 limiter has a more stringent criterion for outgoing fluxes that is violated with this time-varying flow field and time step. When the same set of experiments is performed with smaller time step, this problem does not appear (Fig. 5). It has been found that this problem is alleviated if the maximum Courant number is less than approximately 0.55. Also, the results with and without limiters are very similar (Fig. 5), which implies that limiters have very little effect in this test.

4. Conclusions

We tested the second-order numerical advection method described by Miura (2007) for a number of advection test cases of varying complexity. We find that this numerical method is robust and may be a viable choice for use in global atmospheric models. In addition, three different limiters have been implemented to enforce monotonicity. On comparing results from the numerical simulation of solid-body rotation of a cosine bell with and without limiters, it was found that, by monotonic limiting of the basic numerical scheme, the L_2 error norms are appreciably reduced. As expected, the L_∞ norms increase, which indicates that field extrema are less well captured. In all the cases it was observed that the DK87 limiter (gradient limiting) is the most diffusive and produces the maximum errors in both L_2 and L_∞. The T96 and FCT limiters produce similar results if smaller step sizes are used for model integration, but the FCT limiter appears to be more robust, especially for higher Courant numbers and for more complex or discontinuous flow-field geometries.

Acknowledgments. One of the authors, Rashmi Mittal, thanks the Advance Study Program of the National Center for Atmospheric Research for providing help in the form of a fellowship to carry out this study.

REFERENCES

Dukowicz, J. K., and J. W. Kodis, 1987: Accurate conservative remapping (rezoning) for arbitrary Lagrangian-Eulerian computations. *SIAM J. Sci. Stat. Comput.,* **8,** 305–321.

Lipscomb, W. H., and T. D. Ringler, 2005: An incremental remapping transport scheme on a spherical geodesic grid. *Mon. Wea. Rev.,* **133,** 2335–2350.

Miura, H., 2007: An upwind-biased conservative advection scheme for spherical hexagonal–pentagonal grids. *Mon. Wea. Rev.,* **135,** 4038–4044.

Nair, R. D., and C. Jablonowski, 2008: Moving vortices on the sphere: A test case for horizontal advection problems. *Mon. Wea. Rev.,* **136,** 699–711.

——, J. Cote, and A. Staniforth, 1999: Cascade interpolation for semi-Lagrangian advection over the sphere. *Quart. J. Roy. Meteor. Soc.,* **125,** 1445–1468.

Thuburn, J., 1996: Multidimensional flux-limited advection schemes. *J. Comput. Phys.,* **123,** 74–83.

——, 1997: A PV-based shallow-water model on a hexagonal-icosahedral grid. *Mon. Wea. Rev.,* **125,** 2328–2347.

van Leer, B., 1977: Towards the ultimate conservative difference scheme. IV. A new approach to numerical convection. *J. Comput. Phys.,* **32,** 101–136.

Williamson, D. L., J. B. Drake, J. J. Hack, R. Jakob, and P. N. Swarztrauber, 1992: A standard test set for numerical approximations to the shallow water equation in spherical geometry. *J. Comput. Phys.,* **102,** 211–224.

Yeh, K. S., 2007: The streamline subgrid integration method: I. Quasi-monotonic second-order transport schemes. *J. Comput. Phys.,* **225,** 1632–1652.

Zalesak, S. T., 1979: Fully multidimensional flux-corrected transport algorithms for fluids. *J. Comput. Phys.,* **31,** 335–362.